The Leaky Thermocline

TIMOUR RADKO AND JOHN MARSHALL

Department of Earth, Atmospheric and Planetary Sciences, Massachusetts Institute of Technology, Cambridge, Massachusetts

(Manuscript received 7 February 2003, in final form 12 January 2004)

ABSTRACT

A model for the vertical structure of ocean gyres is presented that extends the ideal thermocline theories of Rhines and Young and Luyten et al. to include a cross-layer volume flux associated with geostrophic eddy transfer. A two-and-one-half-layer model is considered that assumes that the intensity of the eddy transfer depends on the local strength of the current. The ideal thermocline models emerge in the limit where the parameter characterizing the cross-layer volume flux is asymptotically small. Inclusion of the eddy-induced volume flux resolves the nonuniqueness of the Sverdrup dynamics in the unventilated pool attached to the western boundary layer. In the ventilated region, solutions of the model equations converge to their ideal counterparts. The circulation is closed explicitly by developing a western boundary layer theory based entirely on the effects of the cross-isopycnal volume flux due to eddies. Unlike most models of western intensification, the leaky boundary layer here is *active,* and its dynamics are essential for determining the structure of the interior field.

1. Introduction

One of the most influential views on the vertical structure of the subtropical ocean circulation is expressed in the ideal thermocline models (e.g., Luyten et al. 1983; Huang 1988), which assume that the balance in the thermodynamic equation is adiabatic ($\mathbf{v} \cdot \nabla b = 0$, where $\mathbf{v}$ is the velocity and b is the buoyancy) and that fluid particles conserve their density and potential vorticity. Solutions are a mapping of the surface temperature distribution (assumed to be known) to a vertical profile consistent with Sverdrup balance and potential vorticity (PV) conservation. Rhines and Young (1982, RY hereinafter) explained how deep layers that do not outcrop could be set in motion by the slow process of PV transfer across closed geostrophic contours by eddies and resulting PV homogenization. The aforementioned solutions satisfy the Sverdrup constraint and therefore apply only to the ocean interior. Absence of buoyancy and vorticity sinks in these models require an implicit assumption that there is a *passive* nonadiabatic boundary layer that balances the buoyancy and PV budgets but does not affect the interior structure. A number of excellent discussions of thermocline theory include those by Rhines (1986) and Pedlosky (1996).

Although the ventilated thermocline (Luyten et al. 1983) and homogenization (RY) theories are self-consistent models that have brought much insight, one can readily question some of the underlying assumptions. One of the issues (raised by Ierley and Young 1983; IY hereinafter; Luyten and Stommel 1985) is that the perfectly accommodating character of the western boundary layers in the ideal thermocline theories is a feature that should be demonstrated, but not assumed a priori. Another, and perhaps more serious, criticism (e.g., Vallis 2000), is related to our present lack of knowledge of the character and extent of the modification of ideal equations by geostrophic eddies.

In recent papers (Radko and Marshall 2003, 2004; hereinafter RM03, RM04, respectively), we analyzed a set of eddy-resolving numerical simulations of idealized oceanic flows. It was shown that the changes in PV following a Lagrangian particle advected by the mean flow are dominated by the diapycnal buoyancy transfer by eddies, rather than by Reynolds stresses or by explicit diffusion and viscosity. Analogous description of the flow was given in terms of a layered model, in which the eddy buoyancy transfer is represented by a diapycnal volume flux w^*. As discussed in RM03 and RM04, in a continuously stratified fluid w^* can be expressed thus:

$$w^* = w - \frac{Dz(\overline{b})}{Dt} = \frac{-\nabla \cdot (\overline{v'b'}) - B}{\overline{b}_z},$$

where $z(\overline{b})$ is the depth of a mean buoyancy surface, $D/Dt = \overline{u}(\partial/\partial x) + \overline{v}(\partial/\partial y)$, B represents the effects of the small-scale vertical mixing, and $\nabla \cdot (\overline{v'b'})$ is the divergence of the geostrophic eddy buoyancy fluxes. Diagnostics of eddy-resolving numerical simulations in RM03 and RM04 indicate that the intensity of w^* is

Corresponding author address: Dr. Timour Radko, Dept. of Earth, Atmospheric and Planetary Sciences, MIT, Room 54-1517, 77 Massachusetts Avenue, Cambridge, MA 02139.
E-mail: timour@ocean.mit.edu

dominated by the contribution from eddies and is localized to the western intensification zone, where the flow field is characterized by swift currents and small spatial scales.[1]

RM04 demonstrate that the ability of eddies to induce a significant mean cross-isopycnal flux is related to the diabatic component of the eddy fluxes. While eddies are often assumed to be largely adiabatic in the interior (e.g., Gent and McWilliams 1990), numerical simulations indicate that eddies have strong diabatic effects in the near-surface frontal regions, where the presence of the surface tends to suppress the vertical component of the eddy fluxes ($\overline{w'b'}$). Thus, the eddy fluxes become directed across the isopycnals, resulting in large cross-isopycnal fluxes (w^*_{eddy}), which balance, in an integral sense, the downward Ekman flux of buoyant fluid into the main thermocline.

Motivated by these results, we now develop a thermocline model consisting of two active layers overlying an infinitely deep abyssal water. The diapycnal flux w^* is parameterized as a function of local mean flow properties. The present extension of the simple reduced-gravity model in RM03 makes it possible to describe the baroclinic effects, such as active dynamics of the western boundary layers. A fundamental difference between our model and other extensions of ideal thermocline theory (Samelson and Vallis 1997; De Szoeke 1995) is that we attribute the largest part of the diapycnal flux to the action of eddies rather than to small-scale vertical mixing (see the discussion in RM04). This is reflected in the parameterization scheme, which relates the buoyancy fluxes to the lateral, rather than vertical, gradients of the mean field.

The resulting solutions consist of a Sverdrup interior connected to the narrow ''leaky'' western boundary layer. The boundary layer equations are solved explicitly and a complete solution is obtained by matching the interior and boundary layer components. It is shown that the boundary layer is *active* in the sense that it directly controls the pattern of the interior flow. Particular attention is given to a setup (section 3) in which the second layer is completely shielded from the direct influence of wind. This configuration is very similar to that used in RY. However, in contrast to RY, the interior structure in our model is not determined by the slow process of homogenization of potential vorticity, but is set by an interaction of the boundary layer and interior dynamics. The resulting PV distribution is always slightly nonuniform, even when the parameterization of eddies corresponds to a downgradient PV flux. The ventilated model in which the upper-density interface outcrops at the surface is also considered (section 4), and the integral constraints on the eddy-induced diapycnal fluxes are formulated.

[1] Note that w^* here is the total diapycnal volume flux and *not* the vertical eddy-induced velocity of residual mean theory, which is also often denoted by the same symbol.

2. Formulation

Consider a two-and-one-half-layer ocean in a closed rectangular basin. The flow is assumed to be in hydrostatic and geostrophic balance. Geostrophy, assumed for the entire domain (S), implies that the depth of each density interface is constant along the vertical rigid boundaries:

$$h_{\text{dim}}(x, y) = h_{0\,\text{dim}} \qquad (x, y) \in \partial S \quad \text{and}$$
$$D_{\text{dim}}(x, y) = D_{0\,\text{dim}} \qquad (x, y) \in \partial S, \tag{1}$$

where D_{dim} (h_{dim}) is the depth of the lower (upper) interface, and subscript ''dim'' pertains to the dimensional variables. In all cases considered, the lower density interface intersects the basin walls at finite depth ($D_{0,\text{dim}}$), whereas the upper density interface may outcrop at the surface.

The system of nondimensionalization is based on the zonal extent ($L_{x\text{dim}}$) of the basin, the value of the Coriolis parameter at the southern boundary (f_0), and the depth of the lower interface at the basin boundary ($D_{0\text{dim}}$). The corresponding scale of the horizontal velocity is $U = g'D_{0\text{dim}}/f_0L_{x\text{dim}}$, and $P = g'D_{0\text{dim}}$ is used as a scale for the dynamic pressure. Here $g' = g(\Delta\rho_{12}/\rho)$ is the reduced-gravity parameter, and for simplicity, we use equal density differences for both interfaces ($\Delta\rho_{12} = \Delta\rho_{23}$). The resulting steady nondimensional large-scale equations of motion are

$$fv_i = \frac{\partial p_i}{\partial x}, \qquad i = 1, 2,$$
$$fu_i = -\frac{\partial p_i}{\partial y}, \qquad i = 1, 2,$$
$$p_2 = D,$$
$$p_1 - p_2 = h,$$
$$\frac{\partial}{\partial x}(hu_1) + \frac{\partial}{\partial y}(hv_1) + w_e - w_1^* = 0, \quad \text{and}$$
$$\frac{\partial}{\partial x}(h_2u_2) + \frac{\partial}{\partial y}(h_2v_2) - w_2^* + w_1^* = 0, \tag{2}$$

where $h_2 = D - h$ is the depth of the second layer, and w_i^* in the volume equations represent the total diapycnal volume flux due to eddies:

$$w_1^* = -\frac{\partial}{\partial x}(\overline{h'u_1'}) - \frac{\partial}{\partial y}(\overline{h'v_1'}) \quad \text{and}$$
$$w_2^* = -\frac{\partial}{\partial x}(\overline{D'u_2'}) - \frac{\partial}{\partial y}(\overline{D'v_2'}). \tag{3}$$

We assume that this convergence of the ''bolus flux'' is dominated by the contribution from geostrophic eddies that move laterally away from the subtropical gyre and thereby continuously transport light fluid across the isopycnals, analogous to Gulf Stream rings of the North Atlantic subtropical gyre. These eddies detach and even-

tually lose the dynamical influence on the subtropical gyre (see the discussion in RM03, RM04). Of course, the buoyancy of a fluid particle can only be modified by small-scale dissipative processes or direct buoyancy forcing, and therefore the role of eddies in our model is in facilitating the irreversible transfer of properties in their cascade to smaller scales.

The Coriolis parameter varies linearly in y: $f = 1 + \beta y$ in nondimensional units; and Ekman pumping velocity w_e is sinusoidal:

$$w_e(y) = -W_e \sin(\pi y/L_y). \tag{4}$$

Scales are chosen having the North Atlantic subtropical gyre in mind:

$$f_0 = 0.5 \times 10^{-4}\ \mathrm{s}^{-1}, \qquad D_{0\mathrm{dim}} = 10^3\ \mathrm{m},$$

$$L_{x\mathrm{dim}} = 5 \times 10^6\ \mathrm{m}, \qquad g' = 10^{-2}\ \mathrm{m\ s}^2, \quad \text{and}$$

$$W_{e\mathrm{dim}} = 2 \times 10^{-6}\ \mathrm{m\ s}^{-1},$$

in which case the nondimensional Ekman pumping amplitude is about $W_e = 0.2$.

In order to derive an analytical solution that can capture the zero-order physics and dynamics at play, the w_i^* in (2) are parameterized as a function of the local strength of the large-scale flow. Following RM03, we employ a simple and qualitatively plausible thickness diffusion[2] closure:

$$w_1^* = \epsilon\nabla^2 h \quad \text{and} \quad w_2^* = \epsilon\nabla^2 D, \tag{5}$$

where ϵ is related to the dimensional thickness diffusion coefficient (K_{dim}) by $\epsilon = K_{\mathrm{dim}}/UL$.

A coupled system of equations in (D, h) is obtained by eliminating the geostrophic velocities and the dynamical pressure in (2) in favor of the layer depths:

$$\frac{1}{f}J(D, h) - \frac{\beta}{f^2}h\frac{\partial(D+h)}{\partial x} + w_e - w_1^* = 0 \quad \text{and}$$

$$-\frac{1}{f}J(D, h) - \frac{\beta}{f^2}(D-h)\frac{\partial D}{\partial x} - w_2^* + w_1^* = 0, \tag{6}$$

where $J(a, b) = (\partial a/\partial x)(\partial b/\partial y) - (\partial a/\partial y)(\partial b/\partial x)$. An elementary algebraic transformation reduces these equations to

$$-\frac{\beta}{2f^2}\frac{\partial}{\partial x}(h^2 + D^2) + w_e - \epsilon\nabla^2 D = 0 \quad \text{and}$$

$$J\left(D, \frac{D-h}{f}\right) - \epsilon\nabla^2(D-h) = 0, \tag{7}$$

where (5) has been used to parameterize the cross-layer fluxes. Note that (7) is similar to the quasigeostrophic equations with interfacial friction, such as those employed by IY (see appendix A). Here, of course, these equations have a different physical interpretation. The first equation in (7) is essentially Sverdrup balance, modified to take account of finite buoyancy influx into the motionless lower layer. The second equation in (7) describes the Lagrangian variation of potential thickness $R = (D - h)/f$, the reciprocal of the potential vorticity, in the second density layer. In our model the change in potential thickness in (7) is entirely due to eddy-induced cross-isopycnal flux (w^*). Some of our solutions (section 4) are characterized by the outcrop of the first density interface, in which case there is only one active layer in the northern part of the basin. Then (7) reduces to

$$-\frac{\beta}{2f^2}\frac{\partial}{\partial x}D^2 + w_e - \epsilon\nabla^2 D = 0. \tag{8}$$

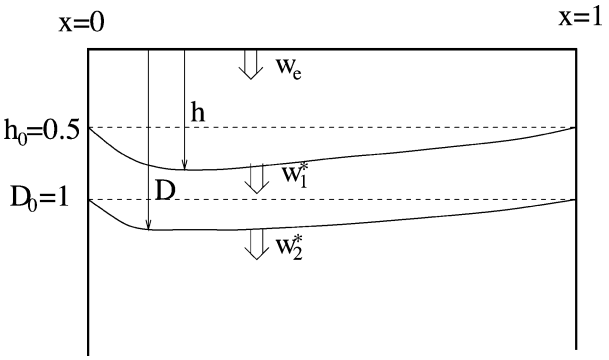

FIG. 1. Schematic of the shielded model. Both density interfaces intersect the boundaries of the rectangular basin at finite depth.

3. Shielded model

a. Numerical solution

Consider the setup in Fig. 1. The second density layer is completely shielded from the direct influence of wind. For simplicity, we assume equal layer depths and therefore set $h_0 = 0.5$. The meridional extent of the basin is $L_y = 0.5$, chosen to roughly approximate the aspect ratio of the North Atlantic subtropical gyre, and the nondimensional beta is $\beta = 1$, so that the Coriolis parameter varies by 50% across the basin. On the basis of the estimates in Marshall et al. (2002) we expect K_{dim} to be on the order of $10^3\ \mathrm{m}^2\ \mathrm{s}^{-1}$, which in our nondimensional units translates to $\epsilon \sim 10^{-3}$–10^{-2}; in the following numerical calculation we use $\epsilon = 3 \times 10^{-3}$.

The nonlinear system (7) has to be solved subject to the boundary conditions $(D, h) = (D_0, H_0)$ at $(x, y) \in \partial S$. One simple and intuitively clear solvability condition for this system appears when the volume equations in (2) are integrated over the total basin area (S) resulting in

[2] A similar parameterization appears in the widely used Gent and McWilliams (1990) model. Gent and McWilliams, however, assume that eddies are adiabatic; because of the prescribed no-flux boundary conditions, the volume of the density layers cannot change in time. In our case, the boundary conditions (1) allow us to represent a fundamentally diabatic effect—the eddy-induced variation in the census of water masses.

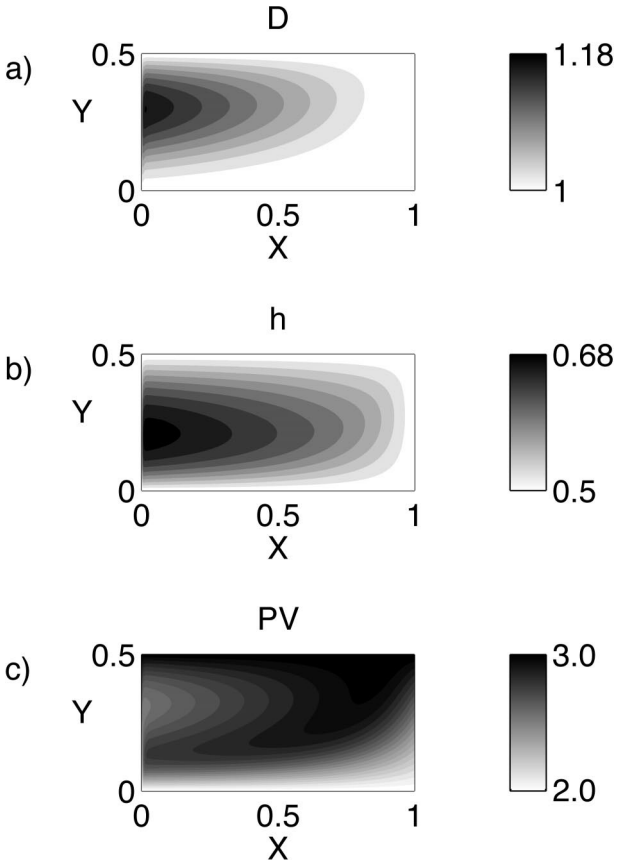

FIG. 2. Depths of the (a) lower and (b) upper density interfaces and (c) second-layer potential vorticity for a steady state obtained by the numerical solution of the governing equations in (2).

$$\int w_e \, dS = \int w_1^* \, dS = \int w_2^* \, dS, \tag{9}$$

which can be interpreted as a requirement that, in a steady state, the continuous flux of buoyancy into each density layer is balanced by the detrainment of warm water by eddies.[3] Note that (9) holds even in the presence of the inertial terms in the momentum equations. Of course, even the existence of a steady state in our problem, and more so its uniqueness or stability, is questionable. Nevertheless, numerical integration of (2) with added time derivatives using a simple finite-difference code yields a steady (for $\epsilon = 3 \times 10^{-3}$) solution, which is presented in Fig. 2.

The structure of the flow in Fig. 2 conforms to our view of the subtropical gyres as consisting of the quasi-adiabatic interior flow smoothly connected to a thin western boundary layer, which in our model is controlled by w^*. The interior field in Fig. 2a includes the shadow zone with almost no motion in the second layer, and a pool region where all streamlines are connected to the boundary layer. Plots of the cross-layer volume fluxes (not shown) reveal the highly localized character of $w_{1,2}^*$, which are confined to the thin western boundary layer in Fig. 2, just as seen in the eddying gyres of RM04. The second-layer potential vorticity in the pool region is slightly nonuniform (Fig. 2c). As will be shown below, this PV distribution is set in our model by an *active* boundary layer, in contrast to the homogenization theory (RY).

Because the solution for small ε is, at the leading order, adiabatic outside of the western boundary layer (see Fig. 2), we briefly review (section 3b) fundamentals of the ideal thermocline theory and then explore the consequences of matching these ideal interior solutions with our ''leaky'' boundary layer.

b. Elements of the ideal thermocline theory

When the small cross-layer fluxes in the interior are neglected, the governing system (7) reduces to the ideal thermocline equations:

$$-\frac{\beta}{2f^2}\frac{\partial}{\partial x}(h^2 + D^2) + w_e = 0 \quad \text{and}$$

$$J\left(D, \frac{D - h}{f}\right) = 0. \tag{10}$$

Integration of the first (Sverdrup) equation in x from the eastern boundary results in an algebraic relationship between D and h:

$$h^2 + D^2 = h_0^2 + D_0^2 + \frac{2f^2}{\beta}(1 - x)W_e \sin\left(\frac{\pi y}{L_y}\right). \tag{11}$$

In order to close the problem and determine a unique distribution of (D, h), one more relation between D and h is needed. The second equation in (10) implies only that D and $R = (D - h)/f$ are functionally related. This is a rather weak requirement that could be satisfied by a whole class of suitable functions, and therefore selection of a specific solution requires an additional constraint on (D, h).

Rhines and Young (1982) pointed out that the functional relation between R and D is fundamentally different in the shadow zone where the PV contours are blocked by the rigid (eastern and northern) boundaries of the basin and in the pool region where the streamlines are closed in a boundary layer (see the schematic in Fig. 3). In the shadow zone, the second-layer flow has to be motionless ($D = \text{const} = D_0$) to satisfy the requirement of no flux normal to the basin boundary, and the Sverdrup transport is entirely in the upper layer. In the pool region, however, the second-layer flow may be finite as long as the potential thickness is a function of the (varying) second-layer depth:

[3] The volumetric balance in (9) should be modified in the presence of the baroclinic cross-gyre exchange flows as in Chen and Dewar (1993). These effects are beyond the scope of the present model.

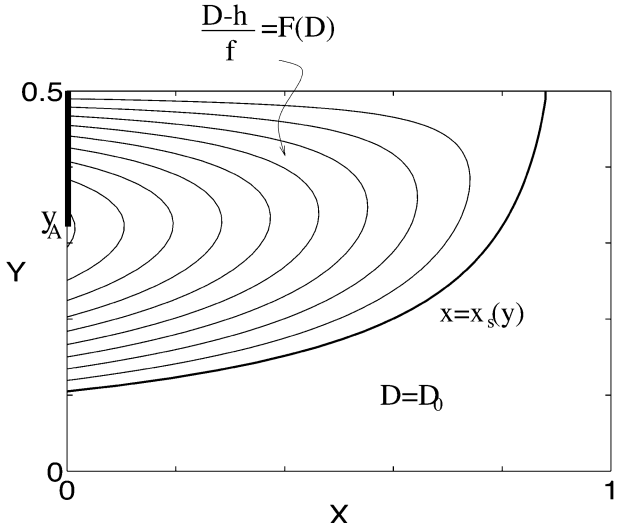

FIG. 3. Structure of the flow field in the second layer. Outside of the narrow western boundary layer isopleths of D coincide with the isopleths of the second-layer potential vorticity $q_2 = f/(D - h)$. Note that $dq_2/dy = 0$ at the return point $y = y_A$.

$$R = \frac{D - h}{f} = F(D). \tag{12}$$

The expression for the boundary $[x = x_s(y)]$ separating these two regions can be obtained by requiring continuity of the depth and constant R along this curve.

The problem, however, is still far from being solved since any function F such that $(D_0 - h_0)/f(L_y) = F(D_0)$ would provide an internally consistent solution of (10). In order to resolve such degeneracy of the ideal equations, RY assumed that the flow is, at leading order, ideal everywhere along each closed streamline and used the higher-order effects to select a particular zero-order solution. Their model becomes particularly simple and intuitively appealing when these higher-order effects result in the downgradient mixing of PV. This process, according to RY, eventually homogenizes PV in the pool region, thereby selecting a unique solution with $F =$ const in (12).

Although relatively homogenized PV regions have been observed in the ocean (McDowell et al. 1982) and in the eddy-resolving numerical experiments (e.g., Rhines and Schopp 1991; Drijfhout and Hazeleger 2001), there is still much controversy regarding the applications of homogenization theory. Dewar (1986), for example, demonstrated how the cross-isopycnal mass exchange can affect the potential vorticity dynamics in the regions shielded from the direct influence of wind, in much the same way as Ekman pumping controls the dynamics of the upper layer. Ierley and Young (1983) pointed out that there is no reason for the homogenization theory to be valid in the presence of a strongly nonadiabatic western boundary layer, and presented a simple counter example—a two-layer quasigeostrophic model with small interfacial and bottom drag. In their model, PV was not homogeneous in the pool region, and in contrast to the assumption in RY, its distribution was set in the frictional boundary layer.

In view of the arguments in IY, a question arises as to how to reconcile their results, which predict the $O(1)$ departure from homogenization, with the existence of zones with relatively uniform PV in the ocean. One possibility is that the process of homogenization *is* the most important factor, and the highly idealized case considered by IY may not be directly relevant to the ocean. Our solution, presented below, suggests an alternative possibility. The mathematical structure of our governing equations (7) is very similar to that in IY (although our interpretation of governing equations is very different). In solving system (7) we essentially revisit the IY problem, but find a very different solution in which the departure from homogenization is rather small, of order 15% (see Fig. 2c). Thus, although we agree with IY's general conclusion about the importance of the boundary layers in setting the interior PV distribution, we question their specific solution (see appendix A).

c. Leaky boundary layers: Passive or active?

To develop a simple analytical description of the steady state in Fig. 2, we search for a solution consisting of an interior part with $O(1)$ scales and the western boundary layer where $\partial/\partial x \gg \partial/\partial y = O(1)$. Because rather low values of ϵ are expected to be realized in the ocean (recall that $\epsilon = 3 \times 10^{-3}$ was used for the experiment in Fig. 2), it is sensible to consider the asymptotic limit $\epsilon \to 0$. In this case the terms with second derivatives in y in (7) become uniformly small everywhere in the basin. In the interior, where $\partial/\partial x = O(1)$ is also assumed, the governing equations in (7) further reduce to the ideal thermocline equations in (10).

The scale for the boundary layer width is obtained by balancing the diffusive terms in (7) with the advective ones:

$$\frac{\partial}{\partial x} \sim \epsilon \frac{\partial^2}{\partial x^2} \to \Delta x = O(\epsilon),$$

and, for convenience, the x coordinate in the boundary layer is rescaled accordingly:

$$x = \epsilon x_0.$$

In the limit $\epsilon \to 0$ the governing equations in (7) reduce to

$$-\frac{\beta}{2f^2}\frac{\partial}{\partial x_0}(h_B^2 + D_B^2) = \frac{\partial^2}{\partial x_0^2} D_B \quad \text{and}$$

$$J_0\left(D_B, \frac{D_B - h_B}{f}\right) = \frac{\partial^2}{\partial x_0^2}(D_B - h_B), \tag{13}$$

where (D_B, h_B) are the interfacial depths in the boundary layer, and $J_0(a, b) = (\partial a/\partial x_0)(\partial b/\partial y) - (\partial b/\partial x_0)(\partial a/\partial y)$.

Since the governing equations are of the second order,

(D_B, h_B) for large x_0 should smoothly merge with the interior solution $[D_I(y), h_I(y)]$ immediately outside of the boundary layer. This requirement can be compactly written as

$$\lim_{x_0 \to \infty} (\hat{D}, \hat{h}) = 0, \tag{14}$$

where $(\hat{D}, \hat{h}) = [D_B(x_0, y) - D_I(y), h_B(x_0, y) - h_I(y)]$ is the difference between the boundary layer and interior solutions.

Consider the transition region of large x_0 where, according to (14), $(\hat{D}, \hat{h}) \ll [D_I(y), h_I(y)]$. When the boundary layer equations in (13) are written in terms of $(\hat{D}, \hat{h})$, $[D_I(y), h_I(y)]$, and only the linear [in $(\hat{D}, \hat{h})$] terms are retained, we obtain

$$-\frac{\beta}{f^2}\frac{\partial}{\partial x_0}(h_I\hat{h} + D_I\hat{D}) = \frac{\partial^2}{\partial x_0^2}\hat{D} \quad \text{and}$$

$$\frac{\partial \hat{D}}{\partial x_0}\frac{\partial}{\partial y}\left(\frac{D_I - h_I}{f}\right) - \frac{\partial D_I}{\partial y}\frac{1}{f}\frac{\partial(\hat{D} - \hat{h})}{\partial x_0} = \frac{\partial^2}{\partial x_0^2}(\hat{D} - \hat{h}). \tag{15}$$

The general solution for this system of linear ordinary (with respect to $\hat{D}$, $\hat{h}$) differential equations is given by

$$\begin{pmatrix}\hat{D}\\ \hat{h}\end{pmatrix} = C_1\begin{pmatrix}1\\ -\dfrac{\lambda_1 f^2}{h_I\beta} - \dfrac{D_I}{h_I}\end{pmatrix}\exp(\lambda_1 x_0) + C_2\begin{pmatrix}1\\ -\dfrac{\lambda_2 f^2}{h_I\beta} - \dfrac{D_I}{h_I}\end{pmatrix}\exp(\lambda_2 x_0) + \begin{pmatrix}C_3\\ C_4\end{pmatrix}, \tag{16}$$

where C_i depend only on y, and $\lambda_i (i = 1, 2)$ are the two roots of the quadratic eigenvalue equation:

$$\lambda^2\frac{f^3}{\beta} + \lambda\left[\frac{f^2}{\beta}\frac{\partial D_I}{\partial y} + (h_I + D_I)f\right] + \left[\frac{\beta}{f}h_I(D_I - h_I) + h_I\frac{\partial h_I}{\partial y} + D_I\frac{\partial D_I}{\partial y}\right] = 0. \tag{17}$$

Requirement (14) immediately sets $C_3 = C_4 = 0$ and the question of whether the remaining two terms are finite depends on the sign of $\mathrm{Re}(\lambda_i)$. If $\mathrm{Re}(\lambda_i) > 0$, then the corresponding term in (16) increases with x_0 and (14) requires C_i to be 0.

The asymptotic behavior of the solution in this transition region indicates whether the boundary layer is *passive*, in the sense that it can be appended to any interior solution, or *active* (e.g., Pedlosky 1996). If both $\mathrm{Re}(\lambda_i)$, $i = 1, 2$, are negative, then for *any* interior flow we can find an appropriate boundary layer solution that would satisfy the boundary conditions at $x_0 = 0$ and smoothly connect to the interior. Consider a different situation when, say, $\mathrm{Re}(\lambda_1) > 0 > \mathrm{Re}(\lambda_2)$. In this case $C_1 = 0$ and there is only one free coefficient (C_2) in (16). Consequently, there is only one degree of freedom to be realized, and a boundary layer solution that would satisfy both matching conditions for D and h cannot be found in general for a given (D_I, h_I). This implies that such a boundary layer is *active* and can directly affect the interior flow by selecting a specific ''preferred'' interior solution.

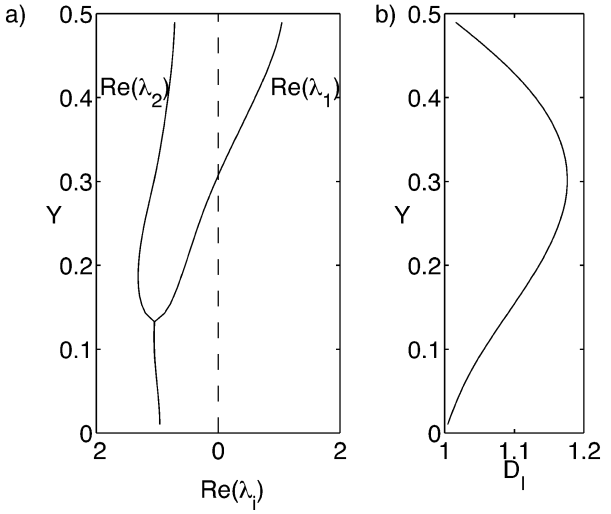

FIG. 4. (a) Solution of the eigenvalue equation in (17). One of the eigenvalues becomes positive in the northern part of the gyre ($y > y_A$), which is indicative of the *active* nature of the boundary layer. (b) Depth of the lower interface immediately outside of the western boundary (D_I) as a function of y. Note that the boundary layer is active wherever the fluid is leaving the boundary and entering the interior $u_I = -(1/f)(\partial D/\partial y) > 0$.

To determine whether our leaky boundary layer is active or passive, we numerically computed the eigenvalues $\lambda_i (i = 1, 2)$ for the flow field in Fig. 2; D_I and h_I were approximated by the values of D and h at the distance $\Delta x = 0.02$ from the western boundary, and the eigenvalues, for each y, were computed using (17). The results in Fig. 4a indicate that in the southern part ($y < y_A = 0.3$) both eigenvalues are negative, $\mathrm{Re}(\lambda_{1,2}) < 0$, which corresponds to a passive boundary layer. However in the northern part of the gyre ($y > y_A$), there is one negative and one positive eigenvalue. Hence, the boundary layer is active, which has a very significant dynamical implication for gyres. It is a first indication that the sought after relation between PV and the stream function in the second layer may be set at the western boundary in the outflow region ($y > y_A$).

It is important to emphasize that the boundary layer becomes active exactly at the location ($y = y_A$) where the second-layer zonal flow reverses its direction (see Fig. 4b). There is a simple theoretical explanation. Recall that the interior flow is assumed to be, at leading order, adiabatic, and the potential thickness is a function of depth in the pool region:

$$\frac{D_I - h_I}{f} = F(D_I).$$

Differentiating this equation in y, we obtain

$$\frac{1}{f}\frac{\partial D_I}{\partial y} - \frac{1}{f}\frac{\partial h_I}{\partial y} - \frac{\beta}{f^2}(D_I - h_I) = F'(D_I)\frac{\partial D_I}{\partial y}. \quad (18)$$

When it is evaluated at the point $y = y_A$, where

$$u_I = -\frac{1}{f}\frac{\partial D_I}{\partial y} = 0, \quad (19)$$

(18) reduces to

$$\frac{1}{f}\frac{\partial h_I}{\partial y} + \frac{\beta}{f^2}(D_I - h_I) = 0 \quad \text{at } y = y_A. \quad (20)$$

Using (19) and (20), we considerably simplify the eigenvalue equation in (17) at $y = y_A$:

$$\lambda^2 + \frac{\beta}{f^2}(h_I + D_I)\lambda = 0 \quad \text{at } y = y_A. \quad (21)$$

The two roots of (21) are

$$\lambda_1 = 0 \qquad \text{at } y = y_A \quad \text{and}$$

$$\lambda_2 = -\frac{\beta}{f^2}(h_I + D_I) \quad \text{at } y = y_A,$$

which shows that λ_1 changes sign (and the boundary layer becomes active) exactly at the same point ($y = y_A$) where the zonal velocity (u_I) reverses its direction.

The ability of the boundary layer to actively control the interior in the northern part of the boundary layer can be rationalized by considering the direction of the Rossby wave propagation immediately outside of the boundary layer. These waves transmit the ''information'' about the remote boundary conditions that affect the interior structure. A simple calculation (not shown) confirms that in the northern part of the pool ($y > y_A$), one of the wave modes is directed eastward, which suggests that the western boundary is active and, hence, can significantly affect the interior structure.

The general suggestion that the interior is controlled by the western boundary layer leads to more specific questions. If the Rhines and Young theory is not relevant for our problem, then what *is* the correct relation between PV and D in the second layer, and how big is the difference between our results and predictions of the homogenization theory? Strong nonlinearity of the governing equations makes it difficult to address these questions on a theoretical level in the most general case. Nevertheless, as we now show, the problem is tractable in two limits: (i) when the Ekman pumping W_e is sufficiently strong, and (ii) when it is sufficiently weak. The precise conditions will be specified below. For now, we mention in passing that the ranges of validity for these two asymptotic limits overlap, and the common parameter range includes the oceanographically relevant scales.

d. Case of strong pumping

The second-layer potential thickness (R) equation for the western boundary region (13) is rewritten as

$$-\frac{\beta}{f^2}\frac{\partial D_B}{\partial x_0}(D_B - h_B) + \frac{1}{f}\frac{\partial D_B}{\partial x_0}\frac{\partial h_B}{\partial y} - \frac{1}{f}\frac{\partial h_B}{\partial x_0}\frac{\partial D_B}{\partial y} = \frac{\partial^2}{\partial x_0^2}(D_B - h_B). \quad (22)$$

To determine the dominant balance in (22), we compare the scales of the first and second terms. Their ratio is

$$\frac{\beta(D_B - h_B)}{f\dfrac{\partial h_B}{\partial y}} \sim \frac{\beta(D_0 - h_0)}{f\dfrac{\Delta h}{\Delta y}} \sim \frac{1}{10}\frac{\beta}{\Delta h}, \quad (23)$$

where Δy is the meridional scale of the return flow from the boundary layer into the interior. The characteristic scale for the variation in the depths of the interfaces (ΔD, Δh) is deduced from the Sverdrup relation (11) for the interior assuming that ΔD and Δh are comparable:

$$\Delta D = (D_{\max} - D_0) \sim \Delta h = (h_{\max} - h_0) \sim \frac{W_e}{\beta}, \quad (24)$$

in apparent agreement with the range of depths observed in Fig. 2.[4]

When (24) is used to simplify (23), it becomes clear that the first term in (22) is negligible if

$$\frac{\beta^2}{10W_e} \ll 1.$$

This scaling argument identifies an important parameter range in which the change in R following a Lagrangian particle passing through the boundary layer is mostly caused by the variation in layer thickness, rather than by meridional variation of the Coriolis parameter. In dimensional units this condition translates to $\beta_{\text{dim}}^2 g' D_{0\text{dim}}^2/(10 f_0^3 W_{e\text{dim}}) \ll 1$. In this regime the boundary layer equations reduce to

$$-\frac{\beta}{2f^2}\frac{\partial}{\partial x_0}(h_B^2 + D_B^2) = \frac{\partial^2}{\partial x_0^2}D_B \quad \text{and}$$

$$-\frac{1}{f}J_0(D_B, h_B) = \frac{\partial^2}{\partial x_0^2}(D_B - h_B). \quad (25)$$

We now search for a solution of this simplified (but still highly nonlinear) system in the *active* part of the boundary layer, $y_A < y < L_y$, where only one boundary condition on (D_B, h_B) could be imposed at $x_0 \to \infty$. The choice of the single boundary condition at infinity is clear. The interior depths (D_I, h_I) are connected by the Sverdrup relation (11), and therefore matching the interior and exterior solutions according to (14) requires that

[4] Strictly speaking, this expression is valid only as long as W_e does not significantly exceed β, and a different scaling appears for $W_e \gg \beta$, but that case will not be discussed herein.

$$\lim_{x_0\to\infty}(h_B^2 + D_B^2) = h_0^2 + D_0^2 + \frac{2f^2}{\beta}W_e \sin\left(\frac{\pi y}{L_y}\right). \quad (26)$$

Boundary conditions at $x_0 = 0$ are given by (1), and these are rewritten below in our boundary layer notation:

$$D_B|_{x_0=0} = D_0 = 1 \quad \text{and} \quad h_B|_{x_0=0} = h_0 = 0.5. \quad (27)$$

Structure of the governing equations in (25) suggests looking for a solution in a form $h_B = D_B + \text{const}$, in which case the second equation in (25) is trivially satisfied. The boundary conditions at $x_0 = 0$ require that

$$h_B = D_B + (h_0 - D_0), \quad (28)$$

and substitution of (28) in the first equation in (25) yields

$$-\frac{\beta}{f^2}\left[\frac{\partial D_B^2}{\partial x_0} - (D_0 - h_0)\frac{\partial D_B}{\partial x_0}\right] = \frac{\partial^2}{\partial x_0^2}D_B.$$

Integrating once in x_0 reduces this equation to

$$-\frac{\beta}{f^2}[D_B^2 - (D_0 - h_0)D_B] = \frac{\partial}{\partial x_0}D_B + \text{const}(y),$$

and the second integration (Abramovitz and Stegun 1964) results in an explicit expression for D:

$$D_B = M\tanh\left[\frac{\beta}{f^2}M(x_0 + N)\right] + \frac{D_0 - h_0}{2}, \quad (29)$$

where $M(y)$ and $N(y)$ are the constants of integration. These constants are determined from the boundary conditions on D_B at $x_0 = 0, \infty$ in (26) and (27):

$$M = \sqrt{\left(\frac{D_0 + h_0}{2}\right)^2 + \frac{f^2}{\beta}W_e \sin\left(\frac{\pi y}{L_y}\right)} \quad \text{and}$$

$$N = \frac{f^2}{\beta M}\tanh^{-1}\left(\frac{D_0 + h_0}{2M}\right).$$

The interior depths (D_I, h_I) are then given by

$$D_I = \frac{D_0 - h_0}{2} + \sqrt{\left(\frac{D_0 + h_0}{2}\right)^2 + \frac{f^2}{\beta}W_e \sin\left(\frac{\pi y}{L_y}\right)} \quad \text{and}$$

$$h_I = \frac{h_0 - D_0}{2} + \sqrt{\left(\frac{D_0 + h_0}{2}\right)^2 + \frac{f^2}{\beta}W_e \sin\left(\frac{\pi y}{L_y}\right)}, \quad (30)$$

which sets a unique relation between the second-layer potential thickness R and the depth of lower interface D.

We now check (for consistency) that the boundary layer is indeed *active* at the origin of all the streamlines in the pool region (see Fig. 3), and therefore (30) determine the flow pattern everywhere in the pool area. As before, we consider the boundary layer transition region (large x_0), and form an eigenvalue equation that describes the asymptotic behavior of the solution in that region:

$$\lambda^2\frac{f^3}{\beta} + \lambda\left[\frac{f^2}{\beta}\frac{\partial D_I}{\partial y} + (h_I + D_I)f\right] + \left(h_I\frac{\partial h_I}{\partial y} + D_I\frac{\partial D_I}{\partial y}\right) = 0. \quad (31)$$

Since the solution (30) is characterized by $\partial h_I/\partial y = \partial D_I/\partial y$, we rewrite (31) in the following form:

$$\lambda^2 + \lambda\left[\frac{1}{f}\frac{\partial D_I}{\partial y} + \frac{\beta}{f^2}(h_I + D_I)\right] + \left[\frac{\beta}{f^2}(h_I + D_I)\frac{1}{f}\frac{\partial D_I}{\partial y}\right] = 0.$$

The two roots of this quadratic equation are

$$\lambda_1 = -\frac{1}{f}\frac{\partial D_I}{\partial y} \quad \text{and} \quad \lambda_2 = -\frac{\beta}{f^2}(h_I + D_I). \quad (32)$$

Although λ_2 is always negative, λ_1 is positive wherever the second-layer flow is directed from the boundary layer into the interior [$u_I = -(1/f)(\partial D_I/\partial y) > 0$] and negative otherwise, confirming that the boundary layer is *active* at the origin of all the streamlines in the pool region.

e. Case of weak pumping

We now turn to the opposite limit of relatively weak Ekman pumping. Recall that the boundary layer equations in (13) reduce to a particularly simple form (15) in the transition region, where the terms that are quadratic in $\hat{D}$, $\hat{h}$ can be neglected. Thus, analytical progress is expected for the parameter regime in which these terms are small everywhere in the boundary layer. To identify the corresponding range of W_e, we rewrite the governing equations in (13) in terms of (D_I, h_I) and ($\hat{D}$, $\hat{h}$):

$$-\frac{\beta}{f^2}\left(h_I\frac{\partial\hat{h}}{\partial x_0} + D_I\frac{\partial\hat{D}}{\partial x_0} + \underline{\hat{h}\frac{\partial\hat{h}}{\partial x_0}} + \underline{\hat{D}\frac{\partial\hat{D}}{\partial x_0}}\right) = \frac{\partial^2}{\partial x_0^2}\hat{D} \quad \text{and}$$

$$-\frac{\beta}{f^2}\frac{\partial\hat{D}}{\partial x_0}(D_I - h_I) - \underline{\frac{\beta}{f^2}\frac{\partial\hat{D}}{\partial x_0}(\hat{D} - \hat{h})} + \underline{\underline{\frac{1}{f}\frac{\partial D_I}{\partial y}\frac{\partial\hat{h}}{\partial x_0}}} - \underline{\underline{\frac{1}{f}\frac{\partial h_I}{\partial y}\frac{\partial\hat{D}}{\partial x_0}}} - \underline{\frac{1}{f}J_0(\hat{D}, \hat{h})} = \frac{\partial^2}{\partial x_0^2}(\hat{D} - \hat{h}). \quad (33)$$

Since $|\hat{D}| < \Delta D$, $|\hat{h}| < \Delta h$ [Δs are defined above in (24)], the criterion for neglecting the terms that are quadratic in ($\hat{D}$, $\hat{h}$) is

$$\Delta D, \Delta h \ll D_0, \quad (34)$$

and these terms are singly underlined in (33).

The range of W_e for this regime is obtained by substituting (24) in (34):

$$\frac{W_e}{\beta} \ll 1, \tag{35}$$

and, apparently, parameters used for the calculation in Fig. 2 ($W_e = 0.2$, $\beta = 1$) satisfy this requirement. A subtle difference between this regime and the widely used quasigeostrophic approximation is that no assumption is made as to the value of β that could be of order 1 in the theory.

Although all the terms underlined in (33) are, formally, of the order $O[(\Delta D)^2]$, analysis of the solution in Fig. 2 indicates that the scales for some of them involve rather large numerical factors $O(10)$. These terms, which are asymptotically small but turn out to be numerically significant, are marked by the double lines in (33) and will be retained in the following analysis. Neglecting the terms underlined only once we immediately recover the linearized set of equations in (15) and (16) discussed in section 3c.

As previously, we concentrate on the *active* part of the boundary layer ($y_A < y < L_y$), in which case the solution (16) reduces to

$$\begin{pmatrix} \hat{D} \\ \hat{h} \end{pmatrix} = C_2 \begin{pmatrix} 1 \\ -\dfrac{\lambda_2 f^2}{h_I \beta} - \dfrac{D_I}{h_I} \end{pmatrix} \exp(\lambda_2 x_0), \tag{36}$$

where λ_2 is the negative root of the eigenvalue equation (17). Boundary conditions on $(\hat{D}, \hat{h})$ at $x_0 = 0$ are

$$\hat{D}|_{x_0=0} = D_0 - D_I \quad \text{and} \quad \hat{h}|_{x_0=0} = h_0 - h_I, \tag{37}$$

and when these are substituted in the general solution (36), we obtain

$$\lambda_2 = -\frac{\beta}{f^2} \frac{D_I(D_0 - D_I) + h_I(h_0 - h_I)}{D_0 - D_I}. \tag{38}$$

The Sverdrup relation (11) immediately outside of the western boundary reduces to

$$h_I^2 + D_I^2 = h_0^2 + D_0^2 + \frac{2f^2}{\beta} W_e \sin\left(\frac{\pi y}{L_y}\right). \tag{39}$$

Differentiation of this relation in y yields

$$h_I \frac{\partial h_I}{\partial y} + D_I \frac{\partial D_I}{\partial y} = \frac{f^2}{\beta} W_e \frac{\pi}{L_y} \cos\left(\frac{\pi y}{L_y}\right) + 2 f W_e \sin\left(\frac{\pi y}{L_y}\right), \tag{40}$$

which we use to simplify the eigenvalue equation in (17). When λ_2 is substituted in (17), the result is an ordinary differential equation in D_I:

$$\frac{\partial D_I}{\partial y} = -\frac{1}{\lambda_2 f^3}\left[\lambda_2^2 f^4 + \beta^2 h_I(D_I - h_I) + f^3 W_e \frac{\pi}{L_y} \cos\left(\frac{\pi y}{L_y}\right) + 2 f^2 \beta W_e \sin\left(\frac{\pi y}{L_y}\right) + \lambda_2 \beta f^2 (h_I + D_I)\right], \tag{41}$$

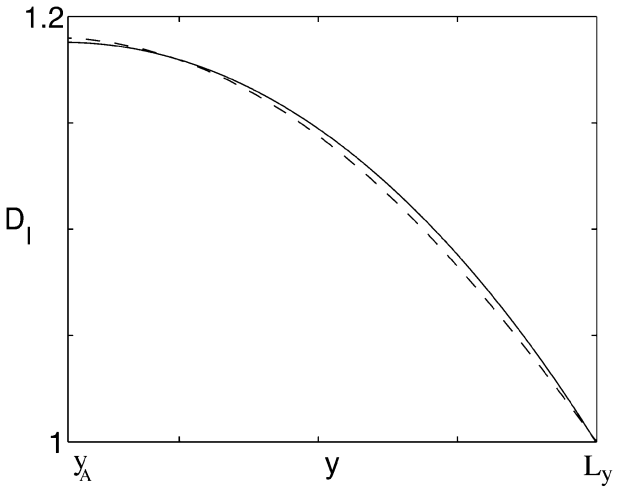

FIG. 5. Comparison of the theoretical (solid line) and numerical (dashed line) solutions for $D_I(y)$ in the northern part of the basin.

which, combined with the expressions for λ_2 in (38) and for h_I in (39), can be integrated in y, given one boundary condition $y = y_A$. The derivation of $[y_A, D_I(y_A), h_I(y_A)]$ is given in appendix B, and for the parameters in Fig. 2, we obtain $y_A = 0.31$, $D_I(y_A) = 1.18$, and $h_I(y_A) = 0.68$, in agreement with the numerical solution in Fig. 2.

Using this boundary condition at y_A we numerically integrate the ordinary differential equation in (41) from $y = y_A$ to $y = L_y$, and the resulting relation $D_I(y)$ is shown in Fig. 5 by solid line. Comparison with the corresponding $D_I(y)$ from the numerical solution of the original equations (dashed line) indicates a very close agreement between the two, thereby supporting our "weak pumping" approximation. Function $D_I(y)$ in the interval $y_A < y < L_y$ determines a unique relation F between the potential thickness and the depth of the lower interface (12) in the pool area. Knowledge of F, in turn, makes it possible to compute the complete solution from the Sverdrup relation

$$[D - fF(D)]^2 + D^2 = D_0^2 + h_0^2 + \frac{2f^2}{\beta}(1 - x) W_e \sin\left(\frac{\pi y}{L_y}\right).$$

This algebraic equation implicitly determines D for each (x, y), although in general it has to be solved numerically.

f. Comparison of the asymptotic and numerical solutions

Each of the two models discussed above has its advantages and limitations. The strong pumping limits yields an explicit analytical solution, whereas the weak pumping model ultimately requires a numerical integration. On the other hand, the formal range of validity for the weak pumping regime (35) seems to better match the oceanographically relevant parameters. In order to

objectively determine which of the two closure schemes is more adequate in resolving the nonuniqueness of Sverdrup dynamics in the pool region, we now compare results of both theories with the numerical solution of the original equations in (2) over a range of W_e.

Since the foregoing boundary layer analysis focused on the relation between the potential thickness (R) and depth (D) in the pool region, we now examine how close our theoretical predictions for $R = F(D)$ are to the corresponding numerical realizations. The scattered dots in (R, D) space in Fig. 6 represent the numerical data from the interior of the pool region. The numerical criterion for specifying the pool area in the numerics has been conveniently (although rather arbitrarily) chosen as

$$(D - D_0) > \frac{1}{4}\Delta D, \qquad x > 0.02.$$

The solid curves in Figs. 6a–c represent the theoretical relation $R = F(D)$ from the weak pumping model, while the predictions from the strong pumping approximation are shown by dashed curves. In all cases considered ($W_e = 0.1, 0.2, 0.3$), the weak pumping theory agrees better with the numerics than does the strong pumping model, as one could have anticipated from their formal ranges of validity (22), (35). Nevertheless, the much simpler analytical ''strong pumping'' model is also able to capture the characteristic features of the numerical $R = F(D)$ dependence, such as an increase in R in the deeper regions of gyre, and explain the relative variation in R over the extent of the pool area.

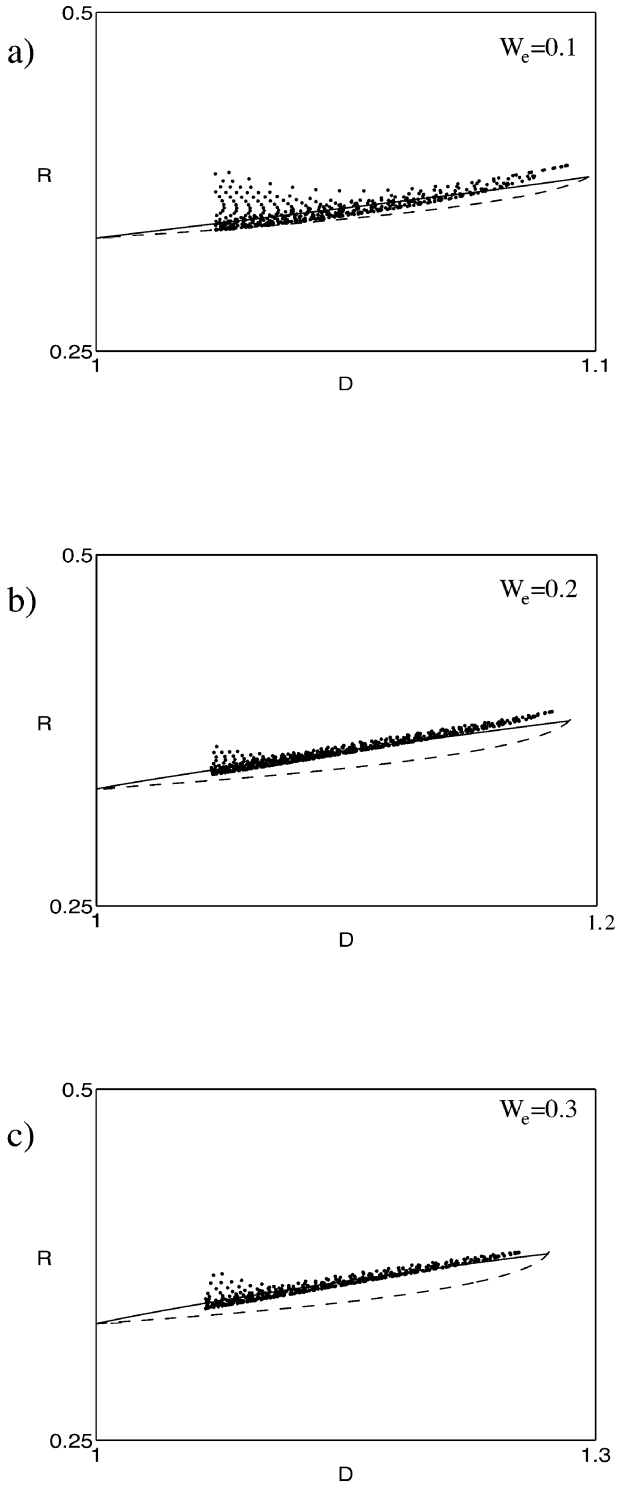

FIG. 6. Comparison of the theoretical predictions for the relation between the potential thickness R and the depth of the lower interface D with the corresponding numerical realizations. Numerical results are shown by dots, solid line corresponds to the weak pumping approximation, and the strong pumping model is shown by dashed line. Nondimensional values of the Ekman pumping velocity are (a) $W_e = 0.1$, (b) $W_e = 0.2$, and (c) $W_e = 0.3$.

g. Downgradient diffusion of potential thickness

In addition to the ''thickness diffusion'' closure used above, we also examine a very important case in which it is assumed that eddies result in a downgradient transfer of the potential thickness (in the quasigeostrophic approximation this is identical to PV diffusion). As we now show, this parameterization results in a very similar solution, also characterized by the active control of the interior flow by the dynamics of the western boundary layer.

In the case of potential thickness diffusion, the Rhines and Young solvability condition, which assumes that the eddy effects are uniformly small along every closed streamline, would trivially yield $R = F(D) = \text{const}$. The RY model is now compared with the results of our analytical theory and numerics. One simple way to achieve a downgradient potential thickness diffusion in our model is to modify the parameterization of the cross-layer buoyancy transfer (5) as

$$w_1^* = \epsilon\nabla^2\left(\frac{h}{f}\right) \quad \text{and} \quad w_2^* = \epsilon\nabla^2\left(\frac{D}{f}\right), \qquad (42)$$

in which case the governing equations reduce to

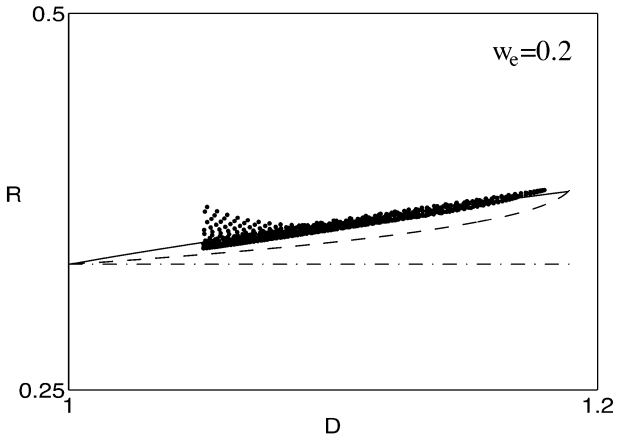

FIG. 7. The same as in Fig. 6 but for the closure (42), which corresponds to the downgradient diffusion of the potential thickness. Numerical results are shown by dots, solid line corresponds to the weak pumping approximation, the strong pumping model is shown by dashed line, and the horizontal dash–dotted line shows the (erroneous) result of the application of the homogenization theory.

$$-\frac{\beta}{2f^2}\frac{\partial}{\partial x}(h^2 + D^2) + w_e - \epsilon\nabla^2\left(\frac{D}{f}\right) = 0 \quad \text{and}$$

$$J\left(D, \frac{D-h}{f}\right) - \epsilon\nabla^2\left(\frac{D-h}{f}\right) = 0. \tag{43}$$

Fortunately, such a modification in the governing equations does not cause any significant changes in our boundary layer theory: the final results of both ''weak'' and ''strong'' pumping models can be reinterpreted to describe the flow governed by (43). This can be readily shown by introducing a new boundary layer variable x_1 defined as

$$x = \frac{\epsilon}{f}x_1.$$

When the boundary layer models are reformulated in terms x_1, it becomes clear that the modification of our theories for the potential thickness diffusion simply involves replacing x_0 in the earlier derivations by x_1. Such an isomorphism is a consequence of the separation between the along- and cross-flow scales in the western intensification zone.

In Fig. 7 we present the $R = F(D)$ relations (i) from the numerical solution of (43), shown by scattered dots; (ii) from the strong and weak pumping models (solid and dashed lines correspondingly); and (iii) by applying the homogenization theory (indicated by horizontal dashed–dotted line). Distribution of the numerical (R, D) points in Fig. 7 clearly favors our boundary layer models, especially the one based on the weak pumping approximation (solid line in Fig. 7). These results conclusively support our main thesis about the *active* control of the boundary layers over the interior PV distribution.

An important question arises as to why the RY mechanism appears to be so inefficient in setting, or even affecting, the PV distribution in the pool region in our numerical calculations. One of the reasons is due to the delicate nature of the homogenization theory. In selecting the particular interior solution, the RY model relies on weak high-order effects. Therefore, as pointed out by Pedlosky (1983), even a very weak violation of the assumptions of the homogenization theory may render it fundamentally invalid. The present model, on the other hand, is based on the leading-order expansion, which generally leads to more robust results. Not surprisingly, it is our zero-order solution that is realized in the numerics for small values of ϵ.

On a more positive note, we would like to point out that the relative variation of PV over the pool area is rather small in our model, about 15% (see Figs. 6, 7). Thus, our results are not inconsistent with the aforementioned observational and numerical evidence for existence of regions with relatively uniform PV. It should be realized, however, that their formation in our model is not caused by the homogenization effect (RY), but is related to the active nature of the western boundary layers.

The scale for the relative variation in the second layer PV can be estimated as follows. In both weak and strong pumping cases (and for both thickness and PV diffusion closures) the solution satisfies a condition $D_I - h_I = D_0 - h_0$ at $y = y_A$. Thus, the difference in PV at $y = y_A$ and $y = L_y$ immediately outside the boundary layer is

$$\Delta\text{PV} = \frac{D_0 - h_0}{f(y_A)} - \frac{D_0 - h_0}{f(L_y)}.$$

Thus, the relative variation in PV over the subtropical gyre is equal to the relative variation of the Coriolis parameter across the width of the return flow $\Delta\text{PV/PV} \sim [f(L_y) - f(y_A)]/f(L_y)$, which is small (~15%) in our idealized models and even less in the ocean.

4. Ventilated model

a. Numerical solution

Consider the model shown in Fig. 8. As previously, the lower interface intersects all the basin boundaries at finite depth $D_0 = 1$, whereas the upper layer is present only in the southern part of the basin: $0 < y < y_h$. Correspondingly, the upper-layer depth vanishes at the southern and zonal boundaries ($h_0 = 0$), and along the outcrop latitude $y = y_h$. Such a setup is probably one of the simplest thermocline models that include the effect of ventilation (Luyten et al. 1983).

Numerical integration of the governing equations in (7) yields a steady solution shown in Fig. 9. Parameters for this run are similar to those used above (section 3): $L_y = 0.5$, $\epsilon = 0.003$, $W_e = 0.2$; the outcrop is located at $y_h = 0.7L_y$. The structure of the flow field is consistent with the classical view (Luyten et al. 1983) of the adi-

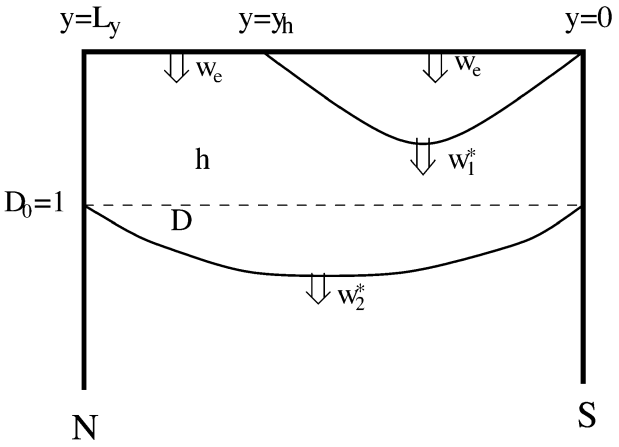

FIG. 8. Schematic diagram for the ventilated model. Meridional cross section.

abatic interior flow sliding along the density interfaces from the surface down into the central thermocline.

For this setup we will not present the detailed mathematical description of the solution, although it should be mentioned that the limit $\epsilon \to 0$ can be treated using the same techniques as employed above for the case of a shielded model (section 3). The major difference between the two models is, of course, in the presence of the ventilated region separating the pool area from the shadow zone. The unique $R = F(D)$ relation in the ventilated region is set at the outcrop latitude ($y = y_h$). For the pool area, we again find that the relation $R = F(D)$ can be deduced from the internal boundary layer dynamics, since the boundary layer there is *active* in the outflow region $y_A < y < y_h$. The only technical complication in deriving an analytical solution for the ventilated model is caused by a meridional boundary layer at the outer edge of the pool area, which results from imposing a downstream boundary condition ($h = 0$ at $y = y_h$) for the northward flow (see Fig. 9b).

b. Integral balances

A principal conceptual value of our idealized solutions is related to their ability to explicitly satisfy some of the key global balances such as appear in the vorticity and buoyancy budgets. Existence of a steady state in our problem implies that the influx of buoyancy in each of density layers is exactly balanced by the detrainment of the warm water by eddies. One can easily confirm this simple idea by integrating the volume equations in (2), which yields, for a setup in Fig. 8,

$$\int_{y<y_h} w_e \, dS = \int_{y<y_h} w_1^* \, dS \quad \text{and}$$

$$\int_{y>y_h} w_e \, dS + \int_{y<y_h} w_1^* \, dS = \int w_2^* \, dS. \tag{44}$$

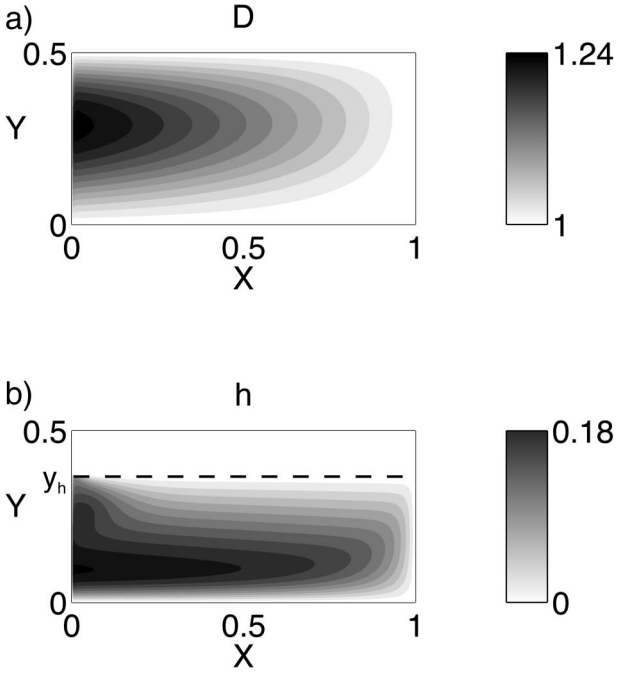

FIG. 9. Depths of the (a) lower and (b) upper density interfaces from the numerics. The first layer is present only in the southern part of the basin ($y < y_h$).

Note that while the Ekman pumping is distributed uniformly in x, the eddy-driven diapycnal fluxes are dramatically intensified to the west. Thus, at the leading order, the interior flow is adiabatic, and the contribution to the integrals in (44) from w_i^* comes mostly from the narrow western boundary layers. It is interesting to note that some structurally similar integral balances were used by Tziperman (1986) to determine the thermocline stratification. However, the diapycnal fluxes in this model were due to the small scale vertical mixing, whereas we discuss, and accordingly parameterize, the eddy-induced diapycnal fluxes—a very different physical process.

A set of important constraints can be derived for the integrals along the closed mean flow contours in each layer. For instance, change in the planetary potential vorticity PV $= f/H$ (H is a thickness of a density layer) at a point advected by a mean flow is caused, in our problem, only by the cross-layer volume fluxes:

$$\frac{D}{Dt}\mathrm{PV} = -\mathrm{PV}\frac{\Delta w^*}{H}, \tag{45}$$

where Δw^* is the diapycnal volume flux per unit area into the layer from both interfaces (see, e.g., Pedlosky 1996). Since, after making a full cycle around the gyre, a Lagrangian particle regains its original PV, the time integral of (45) must be 0. When this simple idea is expressed in terms of the line integrals along the pressure contours C_1 and C_2 in the first and second density layers correspondingly, we obtain

$$\oint_{C_1} \frac{f}{h} w_e |\mathbf{v}_1|^{-1}\, dl = \oint_{C_1} \frac{f}{h_2} w_1^* |\mathbf{v}_1|^{-1}\, dl \quad \text{and}$$

$$\oint_{\substack{C_2 \\ y>y_h}} \frac{f}{D_2} w_e |\mathbf{v}_2|^{-1}\, dl + \oint_{\substack{C_2 \\ y<y_h}} \frac{f}{(D-h)^2} w_1^* |\mathbf{v}_2|^{-1}\, dl$$

$$= \oint_{C_2} \frac{f}{(D-h)^2} w_2^* |\mathbf{v}_2|^{-1}\, dl, \tag{46}$$

and, of course, similar balances could be derived for any function of PV, including such important quantities as the potential enstrophy and potential thickness.

In a companion paper (RM04) we diagnosed a set of numerical models of characteristic oceanic flows and showed that the integral balances discussed in this section (or, more accurately, their continuously stratified counterparts) are indeed realized in the direct eddy-resolving simulations.

5. Conclusions

We have presented a simple two-and-one-half-layer model that extends the classical ideal thermocline theories to include the effects of the cross-layer eddy buoyancy transfer. The intensity of this transfer is not uniform, but depends on the local strength of the mean current allowing a closed solution to be found including a western boundary layer. The resulting steady-state solutions consist of a quasi-adiabatic Sverdrupian interior bounded on the west by a narrow intensification region where most of the buoyancy transfer occurs, which thereby balances the total influx of warm water from the Ekman pumping.

Detailed analysis of the ''leaky'' boundary layers indicates that they are *active* and therefore can directly affect the flow pattern in the gyre interior. Thus, the full solution forms as a result of the interplay between the interior and boundary layer dynamics, in contrast with the commonly accepted notion that the western boundary layers are passive and can be appended to any given interior solution. The flow pattern in our model is characterized the relatively uniform (varying by about 15%) second-layer PV in the pool area attached to the western boundary layer. While the existence of such regions in the ocean and in the numerical simulations is usually related to the homogenization effect (RY), in our model this PV distribution is a direct consequence of the active nature of the boundary layers.

Probably the most questionable assumption of our boundary layer model is related to the neglect of nonlinearity in the momentum equations. This approximation is, however, rather conventional (e.g., Salmon 1986; Samelson and Vallis 1997; Ierley and Young 1986), and the linear model is clearly a prerequisite for developing a complete fully nonlinear theory.

Acknowledgments. We thank the Physical Oceanography division of the National Science Foundation whose support made this study possible. Comments by Eli Tziperman and George Nurser greatly improved the manuscript.

APPENDIX A

Discussion of the Ierley and Young (1983) Model of an Active Boundary Layer

Ierley and Young (1983, hereinafter IY) addressed the question of the active/passive nature of western boundary layers using frictional quasigeostrophic two-layer equations, written (in standard notation) thus:

$$\begin{aligned} J(\psi_1, q_1) &= w_E + \nu\nabla^2(\psi_2 - \psi_1) \\ q_1 &= y + F(\psi_2 - \psi_1), \\ J(\psi_2, q_2) &= \nu\nabla^2(\psi_1 - \psi_2) - \delta\nabla^2\psi_2 \\ q_2 &= y + F(\psi_1 - \psi_2). \end{aligned} \tag{A1}$$

Mathematically, these equations are very similar to those studied in the present paper [see (6) or (7)]. The solution suggested by IY is, however, very different. In our case the flow pattern is characterized by approximately uniform PV in the second layer, whereas IY observe a dramatic departure from homogenization. Thus, an interesting question arises as to the reason for the apparent disagreement between the two models. Below we argue that the cause is a technical flaw in IY.

Ierley and Young (1983) look for a solution in the boundary layer of the form

$$\psi_2 \propto \psi_B, \tag{A2}$$

where $\psi_B = \psi_1 + \psi_2$ is the barotropic streamfunction. Unfortunately, this assumption immediately leads to an internal inconsistency, since the ''*ansatz*'' in (A2) is *incompatible* with the continuous equations of motion (A1). A simple way to demonstrate this is by focusing on the return point y_A where the second-layer interior velocity u_I changes sign. Conservation of the second-layer PV implies that the interior flow immediately outside the boundary layer satisfies a functional relation $q_{2I} = q_{2I}(\psi_{2I})$. Differentiating this in y, we arrive at $(\partial/\partial y)q_{2I} = -(dq_2/d\psi_2)u_I$. Thus, at the return point $[u_I(y_A) = 0]$, any continuous solution should satisfy

$$\frac{\partial}{\partial y} q_{2I}|_{y=y_A} = 0. \tag{A3}$$

That the second-layer PV reaches an extremum at $y = y_A$ is clear even from the topological structure of the PV field (see the schematic in Fig. 3). The *ansatz* in (A2), however, yields $(\partial/\partial y)q_{2I}|_{y=y_A} = 1 + F[(\partial/\partial y)\psi_1 - (\partial/\partial y)\psi_2] = 1$, obviously contradicting the necessary condition (A3).

The *ansatz* in (A2) has further consequences for the theory in IY. The active versus passive character of the

boundary layer can be determined by considering the asymptotic behavior of the solution in the transition region where the boundary layer connects to the ideal interior. We now apply the technique used in section 3 to IY solution. The boundary layer flow is separated into two components: the interior solution immediately outside of the boundary layer $\psi_{1I}(y)$, $\psi_{2I}(y)$ and the residual part $(\hat{\psi}_1, \hat{\psi}_2)$, which varies in x. Linearizing (A1) with respect to $\hat{\psi}_{1,2}$ in the narrow transition region where $\partial/\partial x \gg \partial/\partial y$, we obtain

$$\frac{\partial(\hat{\psi}_1 + \hat{\psi}_2)}{\partial x} = -\delta\frac{\partial^2\hat{\psi}_2}{\partial x^2} \quad \text{and}$$

$$F\frac{\partial\hat{\psi}_2}{\partial x}\frac{\partial\psi_{1I}}{\partial y} - F\frac{\partial\hat{\psi}_1}{\partial x}\frac{\partial\psi_{2I}}{\partial y} + \frac{\partial\hat{\psi}_2}{\partial x} = \nu\frac{\partial^2(\hat{\psi}_1 - \hat{\psi}_2)}{\partial x^2} - \delta\frac{\partial^2\hat{\psi}_2}{\partial x^2}, \tag{A4}$$

which is a direct counterpart of our (15) for the IY problem. The spatial stability characteristics for this linear system are determined by the standard normal mode analysis in which we focus on the modes given by $\hat{\psi}_1 = \psi_{10}\exp(\lambda x)$, $\hat{\psi}_2 = \psi_{20}\exp(\lambda x)$. Consider properties of this system in the vicinity of the return point $y = y_A$, where $\partial\psi_{2I}/\partial y = -u_{2I} \to 0$ and, according to the *ansatz* in (A2), $\partial\psi_{1I}/\partial y$ is also small. The spatial growth rates of the normal modes in (A4) then reduce to

$$\lambda_{1,2} = -\frac{1}{2\nu}(1 + 2\alpha \pm \sqrt{1 + 4\alpha^2}),$$

where $\alpha = \nu/\delta$. Both eigenvalues $(\lambda_{1,2})$ are negative (even for $y > y_A$) which corresponds to the *passive* boundary layer, as explained in section 3.

Thus, the solution in IY cannot be considered a valid conceptual model for an active boundary layer because (i) it violates the equations of motion, and (ii) it describes a fundamentally passive regime, at least in the central part of the pool region.

APPENDIX B

Condition at $y = y_A$ for the Weak Pumping Case

Our goal is to determine, for any given parameters, location of the point y_A that separates the northern active part of the boundary layer from the southern passive part, and the interior depths $[D_I(y_A), h_I(y_A)]$ at this point. As explained in section 3c, two significant events occur at this point. First is the reversal of the second-layer u velocity immediately outside of the western boundary layer:

$$u_I = -\frac{1}{f}\frac{\partial D_I}{\partial y}\bigg|_{y=y_A} = 0, \tag{B1}$$

so that the flow is directed from the boundary layer into interior for $y > y_A$ and into the boundary layer for $y < y_A$. At the same location the eigenvalue λ_1 changes its sign:

$$\lambda_1 = 0, \quad \text{at } y = y_A, \tag{B2}$$

so that in the northern part $(y > y_A)$ there is only one negative eigenvalue, whereas in the southern part both eigenvalues are negative. Substitution of (B1) and (B2) in the eigenvalue equation in (17) results in

$$\frac{\beta}{f}h_I(D_I - h_I) + h_I\frac{\partial h_I}{\partial y} = 0 \quad \text{at } y = y_A. \tag{B3}$$

Equations (B1) and (B3) greatly simplify the eigenvalue equation in (17) at $y = y_A$ resulting in an explicit analytical expression for λ_2:

$$\lambda_2 = -\frac{\beta}{f^2}(h_I + D_I) \quad \text{at } y = y_A. \tag{B4}$$

Comparing (38) and (B4) results in

$$D_I - D_0 = h_I - h_0 \quad \text{at } y = y_A. \tag{B5}$$

When (40) is evaluated at $y = y_A$, we obtain, using (B1), (B3), and (B5),

$$-\frac{\beta}{f}h_I(D_0 - h_0) = \frac{f^2}{\beta}W_e\frac{\partial}{L_y}\cos\left(\frac{\pi y}{L_y}\right) + 2fW_e\sin\left(\frac{\pi y}{L_y}\right) \quad \text{at } y = y_A. \tag{B6}$$

The system of three algebraic equations (39), (B5), and (B6) in three unknowns, y_A, $D_I(y_A)$, and $h_I(y_A)$, can be easily solved numerically for any given parameters. For instance, parameters used in Fig. 2 result in $y_A = 0.31$, $D_I(y_A) = 1.18$, and $h_I(y_A) = 0.68$, in apparent agreement with the numerical solution of the original equations (see Fig. 2).

REFERENCES

Abramovitz, M., and I. A. Stegun, 1964: *Handbook of Mathematical Functions.* Dover, 1046 pp.

Chen, L. G., and W. K. Dewar, 1993: Intergyre communication in a three-layer model. *J. Phys. Oceanogr.,* **23,** 855–878.

De Szoeke, R. A., 1995: A model of wind- and buoyancy-driven ocean circulation. *J. Phys. Oceanogr.,* **25,** 918–941.

Dewar, W. K., 1986: On the potential vorticity structure of weakly ventilated isopycnals: A theory of subtropical mode water maintenance. *J. Phys. Oceanogr.,* **16,** 1204–1216.

Drijfhout, S. S., and W. Hazeleger, 2001: Eddy mixing of potential vorticity versus thickness in an isopycnic ocean model. *J. Phys. Oceanogr.,* **31,** 481–505.

Gent, P. R., and J. C. McWilliams, 1990: Isopycnal mixing in ocean circulation models. *J. Phys. Oceanogr.,* **20,** 150–155.

Huang, R. X., 1988: On boundary value problems of the ideal-fluid thermocline. *J. Phys. Oceanogr.,* **18,** 619–641.

Ierley, G. R., and W. R. Young, 1983: Can the western boundary layer affect the potential vorticity distribution in the Sverdrup interior of a wind gyre? *J. Phys. Oceanogr.,* **13,** 1753–1763.

Luyten, J. R., and H. Stommel, 1985: Upstream effects of the structure of the mid-ocean thermocline. *Progress in Oceanography,* Vol. 14, Pergamon, 387–399.

——, J. Pedlosky, and H. Stommel, 1983: The ventilated thermocline. *J. Phys. Oceanogr.,* **13,** 292–309.

Marshall, J., H. Jones, R. Karsten, and R. Wardle, 2002: Can eddies set ocean stratification? *J. Phys. Oceanogr.,* **32,** 26–38.

McDowell, S., P. Rhines, and T. Keffer, 1982: North Atlantic potential

vorticity and its relation to the general circulation. *J. Phys. Oceanogr.,* **12,** 1417–1436.
Pedlosky, J., 1983: On the relative importance of ventilation and mixing of potential vorticity in mid-ocean gyres. *J. Phys. Oceanogr.,* **13,** 2121–2122.
——, 1996: *Ocean Circulation Theory.* Springer-Verlag, 464 pp.
Radko, T., and J. Marshall, 2003: Equilibration of a warm pumped lens on a β plane. *J. Phys. Oceanogr.,* **33,** 885–899.
——, and ——, 2004: Eddy-induced diapycnal fluxes and their role in the maintenance of the thermocline. *J. Phys. Oceanogr.,* **34,** 372–383.
Rhines, P. B., 1986: Vorticity dynamics of the oceanic general circulation. *Annu. Rev. Fluid Mech.,* **18,** 433–497.
——, and W. R. Young, 1982: A theory of the wind-driven circulation. Part I: Mid-ocean gyres. *J. Mar. Res.,* **40** (Suppl), 559–596.
——, and R. Schopp, 1991: The wind-driven circulation: Quasi-geostrophic simulations and theory for nonsymmetric winds. *J. Phys. Oceanogr.,* **21,** 1438–1469.
Salmon, R., 1986: A simplified ocean circulation theory. *J. Mar. Res.,* **44,** 695–711.
Samelson, R. M., and G. K. Vallis, 1997: Large-scale circulation with small diapycnal diffusion: The two-thermocline limit. *J. Mar. Res.,* **55,** 223–275.
Tziperman, E., 1986: On the role of interior mixing and air–sea fluxes fin determining the stratification and circulation of the oceans. *J. Phys. Oceanogr.,* **16,** 680–693.
Vallis, G. K., 2000: Thermocline theories and WOCE: A mutual challenge. *Int. WOCE Newsletter,* No. 39, WOCE International Project Office, Southampton, United Kingdom, 30–33.